Synthesis and Characterization of Manganese Ferrite Nanoparticles by Thermal Treatment Method

ARTICLE *in* JOURNAL OF MAGNETISM AND MAGNETIC MATERIALS · JULY 2011

Impact Factor: 1.97 · DOI: 10.1016/j.jmmm.2011.01.016

Journal of Magnetism and Magnetic Materials 323 (2011) 1745–1749

Contents lists available at ScienceDirect

Journal of Magnetism and Magnetic Materials

journal homepage: www.elsevier.com/locate/jmmm

Synthesis and characterization of manganese ferrite nanoparticles by thermal treatment method

M. Goodarz Naseri [a,b,*], E. Bin Saion [a], H. Abbastabar Ahangar [c], M. Hashim [a,d], A.H. Shaari [a]

[a] Department of Physics, Universiti Putra Malaysia, 43400 UPM Serdang, Selangor, Malaysia
[b] Department of Physics, Faculty of Science, Malayer University, Malayer, Iran
[c] Department of Chemistry, Universiti Putra Malaysia, 43400 UPM Serdang, Selangor, Malaysia
[d] Advance Materials and Nanotechnology Laboratory, Institute of Advanced Technology, University Putra Malaysia, 43400 UPM, Serdang, Selangor, Malaysia

ARTICLE INFO

Article history:
Received 13 October 2010
Received in revised form
9 January 2011
Available online 2 February 2011

Keywords:
Manganese ferrite
Nanoparticle
Thermal treatment
Magnetic property

ABSTRACT

Cubic structured manganese ferrite nanoparticles were synthesized by a thermal treatment method followed by calcination at various temperatures from 723 to 873 K. In this investigation, we used polyvinyl pyrrolidon (PVP) as a capping agent to control the agglomeration of the nanoparticles. The characterization studies were conducted by X-ray diffraction (XRD) and transmission electron microscopy (TEM). The average particle sizes of manganese ferrite nanoparticles were determined by TEM, which increased with the calcination temperature from 12 to 22 nm and they had good agreement with XRD results. Fourier transform infrared spectroscopy confirmed the presence of metal oxide bands at all temperatures and the absence of organic bands at 873 K. Magnetic properties were demonstrated by a vibrating sample magnetometer, which showed a super-paramagnetic behavior for all samples and also saturation magnetization (M_s) increases from 3.06 to 15.78 emu/g by increasing the calcination temperature. The magnetic properties were also confirmed by the use of electron paramagnetic resonance spectroscopy, which revealed the existence of unpaired electrons and also measured peak-to-peak line width, resonant magnetic field and the g-factor.

1. Introduction

Recently, many studies have focused on the synthesis of nanomaterials, such as spinel ferrite nanocrystals, which have attracted much attention because of their surface effect (large surface-to-volume ratio) and quantum confinement effects (size-dependent properties). These factors affect their physical and chemical properties. Magnetite and spinel ferrite nanocrystals are regarded as two of the most important inorganic nanomaterials because of their electronic, optical, electrical, magnetic, and catalytic properties, all of which are different from the properties of their bulk counterparts. Spinel ferrites have the structure AB_2O_4 in which A and B display tetrahedral and octahedral cation sites, respectively, and O indicates the oxygen anion site [1]. Among spinel ferrites, manganese ferrite ($MnFe_2O_4$) nanoparticles are very important because they have proven to be useful in many magnetic applications, such as recording media devices [2], drug delivery [3], ferrofluid [4], biosensors [5], and contrast-enhancement agents for MRI technology [6]. The properties of manganese ferrite nanoparticles are dependent on their micro-structural characteristics, i.e., particle size and shape, which can be controlled in the fabrication processes. In order to achieve materials of the desired physical and chemical properties, the preparation of manganese ferrite nanocrystals through different routes has become an essential part of related research and development activities. Various fabrication methods to prepare spinel manganese ferrite nanocrystals have been reported, including the sol–gel method [7], co-precipitation [8], reverse micelles [9], and the hydrothermal method [10]. Various precipitation agents have been used to produce manganese ferrite nanocrystals of a specific size and shape, e.g., metal hydroxide in the co-precipitation method, surfactant and ammonia in the reverse micelles and micro-emulsion methods, organic matrices in the sol–gel method, and high temperature and pressure in the hydrothermal method. Most of these methods have achieved particles of the required size and shape, but they are impractical for large-scale applications because of they require expensive and complicated procedures, high reaction temperatures, long reaction times, and toxic reagents. They also produce toxic by-products that may harm the environment. In the present study, manganese ferrite nanocrystals were prepared using a thermal treatment method in an aqueous solution containing metal nitrates, polyvinyl pyrrolidone, and deionized water, followed by grinding and calcination.

* Corresponding author at: Department of Physics, Universiti Putra Malaysia, 43400 UPM Serdang, Selangor, Malaysia. Tel.: +601 42698153; fax: +603 89454454.
E-mail address: mahmoud.naseri55@gmail.com (M. Goodarz Naseri).

0304-8853/$ - see front matter © 2011 Elsevier B.V. All rights reserved.
doi:10.1016/j.jmmm.2011.01.016

No other chemicals were added to the solution. This method offers the advantages of simplicity, low cost, and low reaction temperatures; in addition, it is environment-friendly as it produces no by-product effluents. It must be mentioned that the main drawbacks of this method are removal of PVP and simultaneously controlling particle size of ferrite, moreover it is still limited to some of the materials. The textural and morphological characteristics of the manganese ferrite nanocrystals were studied with various techniques to verify the influence of calcination temperature on the crystallization, morphology, and particle size distribution of the nanocrystals, as well as to explore other parameters of interest.

2. Experimental

Metal nitrate reagents were used as precursors, polyvinyl pyrrolidone (PVP) was used as the capping agent, and deionized water was used as the solvent. Iron nitrate, $Fe(NO_3)_3 \cdot 9H_2O$, and manganese nitrate, $Mn(NO_3)_2 \cdot 6H_2O$, were purchased from Acros Organics with purities exceeding 99%. PVP (MW=29,000) was purchased from Sigma Aldrich and was used without further purification. An aqueous solution of PVP was prepared by dissolving the polymer in 100 ml of deionized water at 343 K; then, 0.2 mmol of iron nitrate and 0.1 mmol of manganese nitrate (Fe:Mn=2:1) were placed in the polymer solution, which was stirred for 2 h using a magnetic stirrer. At the end of the 2 h period, a colorless, transparent solution was obtained. Using a glass electrode, the pH of the solution was determined to be in the range 1–2. No precipitation of materials was observed before the heat treatment. The solution was poured into a glass Petri dish and heated in an oven at 353 K for 24 h to evaporate the water. The dried, orange, solid manganese ferrite that remained was crushed and ground in a mortar to form powder. The calcinations of the powder were conducted at 723, 773, 823, and 873 K for 3 h to decompose the organic compounds and crystallize the nanocrystals.

3. Characterization

The structure of the $MnFe_2O_4$ nanoparticles was characterized by the XRD technique, using a Shimadzu diffract meter model XRD 6000 employing Cu K_α (0.154 nm) radiation to generate diffraction patterns from powder crystalline samples at an ambient temperature in 2θ range of 10°–80°. The microstructure and particle size of the nanocrystals were determined from Transmission Electron Microscopy (TEM) images obtained using a JEOL 2010F UHR version electron microscope at an accelerating voltage of 200 kV. FT-IR spectra were recorded using a PerkinElmer FT-IR spectrometer, model 1650. Before recording spectra, the samples were placed on a Universal ATR Sampling Accessory (diamond coated with CsI) and pressed, and then the spectra were recorded. Magnetization measurements were conducted using a vibrating sample magnetometer (VSM) (Lake Shore 4700) at room temperature with a maximum magnetic field of 15 kOe. Electron paramagnetic resonance (EPR) spectra were recorded on a JEOL JES-FA200 EPR spectrometer (JEOL, Tokyo, Japan) at room temperature.

4. Results and discussion

The interactions between PVP and metal ions are represented schematically in Fig. 1, which shows that the manganese (II) and iron (III) ions are bound by strong ionic bonds between the metallic ions and the amide group in a polymeric chain or between the polymeric chains. This uniform immobilization of

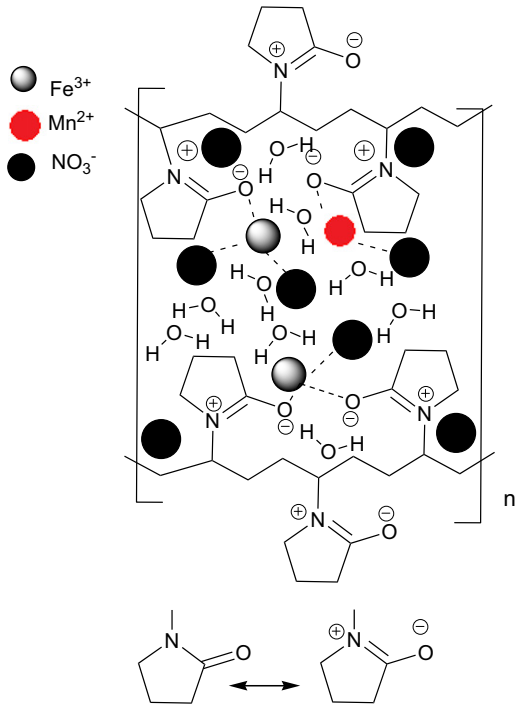

Fig. 1. A proposed mechanism of interactions between PVP and metal ions.

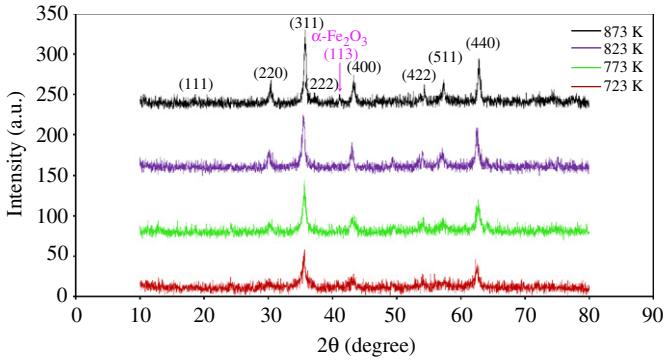

Fig. 2. XRD patterns of manganese ferrite nanoparticles calcined at different temperatures. (For interpretation of the references to color in this figure, the reader is referred to the web version of this article.)

metallic ions in the cavities of the polymer chains favors the formation of a uniformly-distributed, solid solution of the metallic oxides in the calcination process.

The XRD diffraction patterns of the manganese ferrite nanoparticles (JCPDS, 73-1964) are shown in Fig. 2. The patterns show the reflection planes (1 1 1), (2 2 0), (3 1 1), (2 2 2), (4 0 0), (4 2 2), (5 1 1), (4 4 0), and (5 3 1), which confirm the presence of single-phase $MnFe_2O_4$ with a face-centered cubic structure [11]. The appearance of the plane (1 1 3) is due to the formation of the α-Fe_2O_3 phase at 873 K (as shown with pink color in Fig. 2), which is evidence of the transfer of Fe^{3+} ions from B site to A site in the mixed spinel structure of $MnFe_2O_4$ nanoparticles. A neutron diffraction experiment performed on the mixed spinel structure of $MnFe_2O_4$ nanoparticles showed the existence of Mn^{2+} and Fe^{3+} ions in the sub-lattices of A and B [9].

The average particle size was determined from the full width at half maximum (FWHM) using the well-known Debye–Scherrer equation

$$D = 0.9\lambda/\beta\cos\theta$$

Table 1
Average particle size (nm) of $MnFe_2O_4$ nanoparticles determined from XRD and TEM and magnetic properties observed from VSM and ESR techniques at room temperature for samples calcined at 723, 773, 823, and 873 K.

$MnFe_2O_4$ nanoparticles	Temperature (K)	XRD (nm)	TEM (nm)	M_s (emu/g)	Line width ΔH_{pp} (Oe)	Gyromagnetic ratio (g)	H_r (Oe) Resonance field
MnFerrite 1	723	15	12 ± 4	3.06	–	–	–
MnFerrite 2	773	17	15 ± 2	6.31	910	2.1252	2989
MnFerrite 3	823	20	17 ± 5	7.96	970	2.1307	2977.5
MnFerrite 4	873	23	22 ± 4	15.78	1470	2.1601	2976

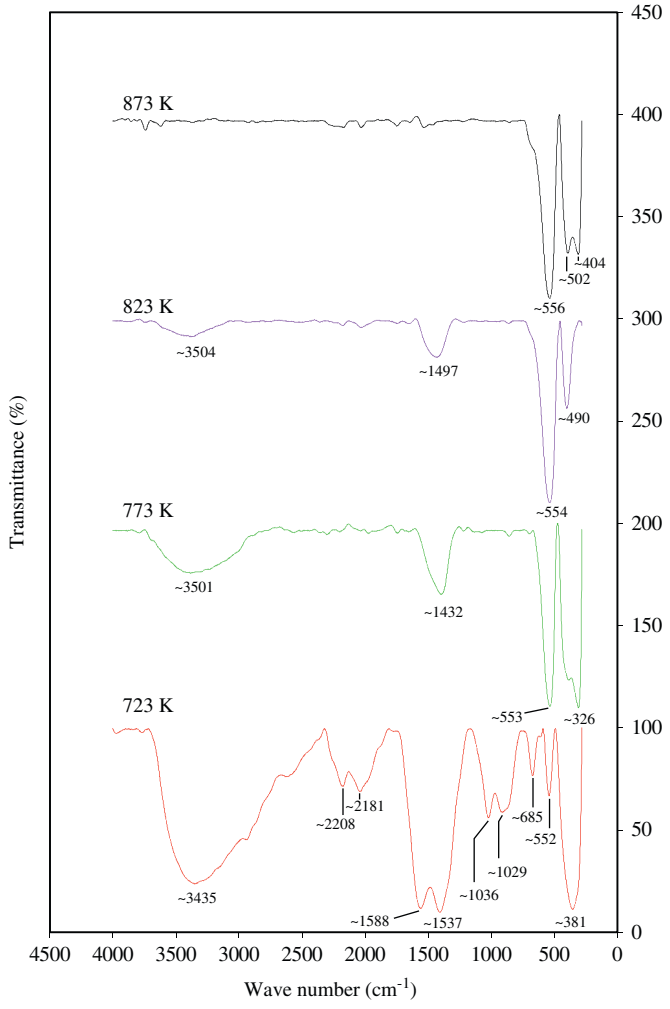

Fig. 3. FT-IR spectra of manganese ferrite nanoparticles calcined at different temperatures.

where D is the crystallite size (nm), β is the full width of the diffraction line at half the maximum intensity measured in radians, λ is X-ray wavelength of Cu K_α=0.154 nm, and θ is the Bragg angle [12]. Our results showed that, as the calcination temperature increased, the diffraction peaks became sharper and narrower and increased in intensity [11]. The crystallite sizes estimated using the Debye–Scherrer equation were found to increase with the calcination temperature, from about 12 nm at 723 K to 22 nm at 873 K, as shown in Table 1.

The manganese ferrite samples were studied further for the interaction between the formation of crystalline $MnFe_2O_4$ nanostructures and the PVP matrix at different calcination temperatures using FT-IR spectra analysis (Fig. 3). The FT-IR spectra illustrate that absorption bands of Mn–O and Fe–O bonds appeared at 404, 502, and 556 cm^{-1}, respectively, for pure spinel manganese ferrite that was calcined at 873 K. (Fig. 3 at 873 K). These bonds provide evidence of the formation of the metal ions-oxygen in the tetrahedral and octahedral sites in the spinel structure, as suggested by previously published data [13]. The IR bands of solids are usually assigned to the vibration of ions in the crystal lattice. The absence of the peaks in the range of 1000–1300 cm^{-1} and 2000–3000 cm^{-1} in the calcined sample at 873 K confirmed that the O–H mode, C–O mode, and C=H stretching-mode of organic sources did not exist [14].This IR analysis was very useful for establishing the temperature of calcination at 873 K by removing unwanted ions that can pollute the crystal lattice during preparation. At the lower temperature of 873 K, however, there were still traces of broadband absorption peaks at 1497 and 3504 cm^{-1} due to traces of adsorbed or atmospheric CO_2 and O–H stretching vibration, respectively (Fig. 3 at 823 K) [15].

The TEM images in Fig. 4 show the size, shape, and distribution of manganese ferrite samples at different calcination temperatures from 723 to 873 K. The results indicate that the samples prepared by the thermal treatment method are uniform in morphology and particle size distribution. The particle size was increased by increasing the calcination temperature (Table 1). The smallest particle size obtained in this study was 12 nm at 723 K and it reached 22 nm at the highest calcination temperature of 873 K. This suggests that several neighboring particles fuse to increase the particle sizes by the melting of their surfaces [16]. A grain growth of particle size enlargement at higher calcination temperatures was observed previously in nickel ferrite [17] and in cobalt ferrite [18] systems.

Fig. 5 shows the curves of magnetization that were measured at room temperature in range of approximately −15 to +15 kOe, which exhibit super-paramagnetic behaviors. Table 1 depicts the values of saturation magnetization (M_s) of different samples. When the calcination temperature increased from 723 to 873 K, the saturation magnetization increased from 3.06 to 15.78 emu/g. This can be attributed to spin canting and surface spin disorder that occurred in these nanoparticles [19,20].

The interactions between A and B sub-lattices in the spinel lattice system (AB_2O_4) consist of inter-sub-lattice (A–B) super-exchange interactions and intra-sub-lattice (A–A) and (B–B) exchange interactions. Inter-sub-lattice super-exchange interactions of the cations on the (A–B) are much stronger than the (A–A) and (B–B) intra-sub-lattice exchange interactions [21,22].

As discussed earlier (Fig. 2), by increasing the calcination temperature of the $MnFe_2O_4$ nanoparticles, Fe^{3+} ions transferred from B site to A site, so the accumulation of Fe^{3+} ions increased in A site; however, the Fe_A^{3+}–Fe_B^{3+} super-exchange interactions increased (Fe_A^{3+}–Fe_B^{3+} interactions were twice as strong as the Mn_A^{2+}–Fe_B^{3+} interactions), and this can lead to an increase in saturation magnetization in $MnFe_2O_4$ nanoparticles [7]. Aslibeiki et al. [23] showed that saturation magnetization increases with increasing temperature and particle size in $MnFe_2O_4$ nanoparticles.

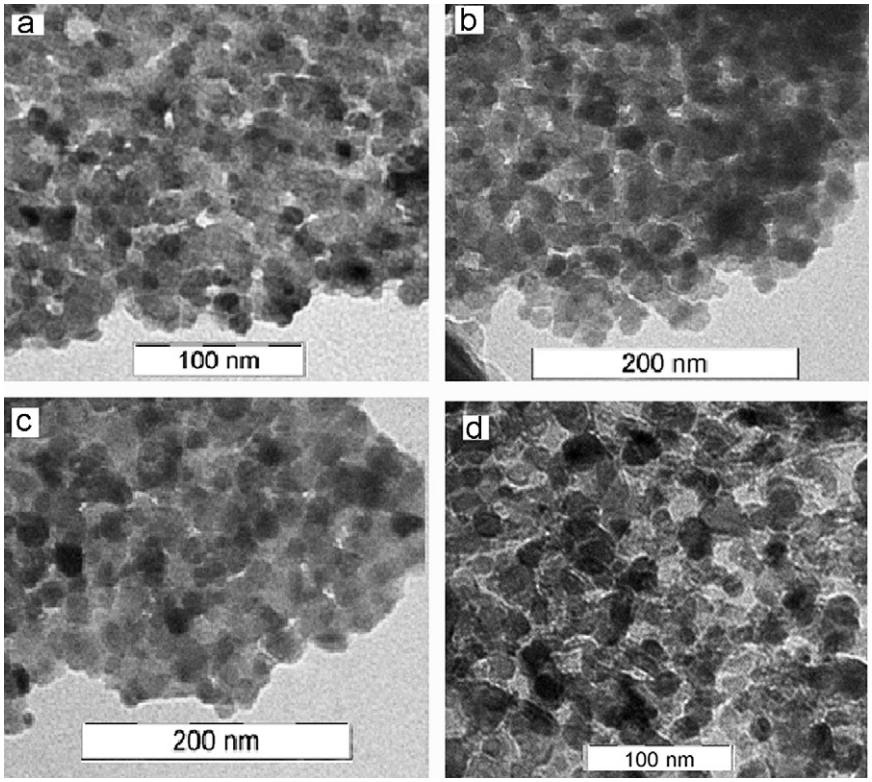

Fig. 4. TEM images of manganese ferrite nanoparticles calcined at (a) 723, (b) 773, (c) 823, and (d) 873 K.

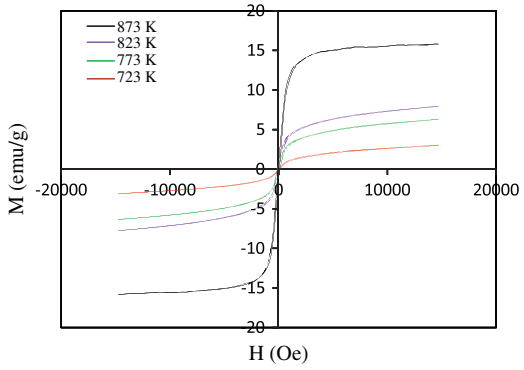

Fig. 5. VSM curves of manganese ferrite nanoparticles calcined at different temperatures.

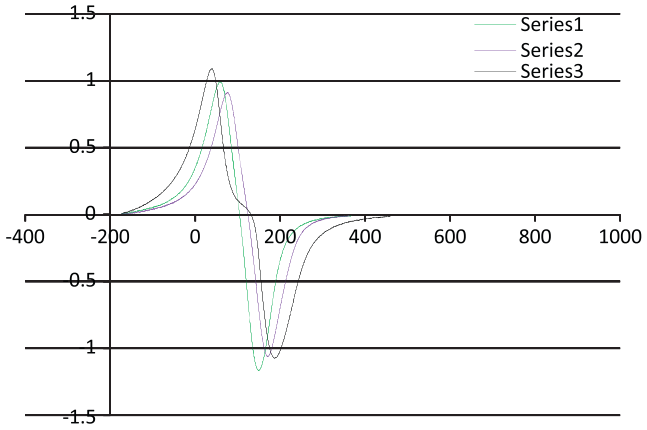

Fig. 6. EPR spectra of manganese ferrite nanoparticles calcined at different temperatures.

It has been reported [24] that the spin disorder may occur on the surface of the nanoparticles as well as within the cores of the nanoparticles due to vacant sub-lattice disorder sites (Fe_A^{3+}) and poor crystal structure. The other point that is understood from Fig. 5 is that the values of saturation magnetization are expressively lower than those reported for the bulk $MnFe_2O_4$ (80 emu/g) [25]. The decrease in saturation magnetization of all the samples compared to that of the bulk is ascribed to the surface effects in these nanoparticles. The existence of an inactive magnetic layer or a disordered layer on the surfaces of the nanoparticles can be due to the decrease of saturation magnetization compared to the bulk value [18,26,27]. It is worth mentioning that the preparation and synthesis processes are apart from the particle size. For instance, saturation magnetization of the 3-nm manganese ferrite made by co-precipitation [28] gives a value of about 13 emu/g at room temperature, whereas, 4-nm manganese ferrite made by the reverse micelles [29] gives 30 emu/g of saturation magnetization for similar conditions.

The EPR spectra of the samples calcined at room temperature are shown in Fig. 6. All spectra exhibited broad and symmetrical signals. Peak-to-peak line width (ΔH_{pp}), resonant magnetic field (H_r), and g-factor are three parameters that characterize the magnetic properties [30]. It is obvious from Table 1 that the values of ΔH_{pp} increase from 910 to 1470 Oe and the values of g-factor increase from 2.12 to 2.16 when the calcination temperature and particle size were increased. This suggests that microscopic magnetic interactions increase as particle size increases. In ferrites, variations of ΔH_{pp} and g-factor can be due to dipole-dipole interactions and super-exchange interactions [31].

Table 1 shows that the value of the resonant magnetic field decreases from 2989 to 2976 Oe as the calcination temperature increases. According to the equation

$$g = h\nu/\beta H$$

where h is Planck's constant, ν is the microwave frequency, β is the Bohr magneton (9.274×10^{-21} erg Oe^{-1}) and H is resonant magnetic field, the resonance magnetic field should decrease when g-factor increases, whereas ν is constant in EPR spectroscopy. The addition of Fe^{3+} ions at higher temperature in A site causes an increase in the super-exchange interactions, contributing to an increase in the internal field and a decrease in the resonance magnetic field [13]. Increases in ΔH_{pp} and g-factor and decreases in H_r with increase in calcination magnetization values have been reported in $NiFe_2O_4$ nanoparticles [17].

5. Conclusion

Spinel manganese ferrite ($MnFe_2O_4$) nanocrystals were synthesized by a thermal treatment method. As confirmed by XRD and TEM analyses, particle sizes ranging from 12 to 22 nm were achieved with calcination temperatures between 723 and 873 K. Calcination at 873 K with an average particle size of 22 ± 4 nm completely eliminated organic compounds and confirmed the existence of metal oxide bands at all calcination temperatures. Manganese ferrite demonstrated a super-paramagnetic behavior and increased saturation as temperature increased. Electron paramagnetic resonance (EPR) spectroscopy was used to measure the peak-to-peak line width (ΔH_{pp}), resonant magnetic field (H_r), and the g-factor values. This simple, cost-effective, and environment-friendly method, which has low reaction temperatures and produces no by-product effluents, can be used to fabricate pure, crystalline spinel manganese ferrite nanocrystals. Furthermore, this method can be extended to fabricate other spinel ferrite nanoparticles of interest.

Prime novelty statement

This paper highlights the synthesis of manganese ferrite nanoparticles from metallic nitrates, PVP, and deionized water by thermal treatment at 353 K for 24 h followed by crushing and calcinations. No other chemicals were added in this process.

Acknowledgments

The authors would like to thank Miss. Fatemeh Moazami Goodarzi for her great assistance in the chemical mechanism study. This work was supported by the Ministry of Higher Education of Malaysia under the FRGS grant and Universiti Putra Malaysia under the RUGS grant.

References

[1] R.C.O. Handley, Modern Magnetic Materials: Principles and Applications, NewYork, John Wiley & Sons, 2000.
[2] S.R. Ahmed, S.B. Ogale, G.C. Papaefthymiou, R. Ramesh, P. Kofinas, Magnetic properties of $CoFe_2O_4$ nanoparticles synthesized through a block copolymer nanoreactor route, Appl. Phys. Lett. 80 (2002) 1616–1618.
[3] I. Brigger, C. Dubernet, P. Couvreur, Nanoparticles in cancer therapy and diagnosis, Adv. Drug Delivery Rev. 54 (2002) 631–651.
[4] R. Arulmurugan, G. Vaidyanathan, S. Sendhilnathan, B. Jeyadevan, Mn-Zn ferrite nanoparticles for ferrofluid preparation: study on thermal-magnetic properties, J. Magn. Magn Mater. 298 (2006) 83–94.
[5] J.B. Haun, T.J. Yoon, H. Lee, R. Weissleder, Magnetic nanoparticle biosensors, Wiley Interdiscip. Rev. Nanomed. Nanobiotechnol. 2 (2010) 291–304.
[6] D. Portet, B. Denizot, E. Rump, J. Lejeune, P. Jallet, Nonpolymeric coatings of iron oxide colloids for biological use as magnetic resonance imaging contrast agents, J. Colloid Interf. Sci. 238 (2001) 37–42.
[7] L. Jianjun, Y. Hongming, L. Guodong, L. Yanju, L. Jinsong, Cation distribution dependence of magnetic properties of sol–gel prepared $MnFe_2O_4$ spinel ferrite nanoparticles, J. Magn. Magn Mater. 322 (2010) 3396–3400.
[8] J. Amighian, M. Mozaffari, B. Nasr, Preparation of nano-sized manganese ferrite ($MnFe_2O_4$) via coprecipitation method, Phys. Status Solidi C 3 (2006) 3188–3192.
[9] C. Liu, B. Zou, A.J. Rondinone, Z.J. Zhang, Reverse Micelle Synthesis and Characterization of Superparamagnetic $MnFe_2O_4$ Spinel Ferrite Nanocrystallites, J. Phys. Chem. B 104 (2000) 1141–1145.
[10] D. Zhang, X. Zhang, X. Ni, J.M. Song, H. Zheng, Low-temperature fabrication of $MnFe_2O_4$ octahedrons: magnetic and electrochemical properties, Chem. Phys. Lett. 426 (2006) 120–123.
[11] J.P. Singh, R.C. Srivastava, H.M. Agrawal, R.P.S. Kushwaha, 57Fe Mössbauer spectroscopic study of nanostructured zinc ferrite, J. Hyperfine Interact. 183 (2009) 393–400.
[12] D. Cullity, Elements of X-ray Diffraction, 2nd ed., Addison-Wesley, London, 1978.
[13] A. Pradeep, P. Sambasiva Rao, G. Chandrasekaran, P. Priyadharsini, Structural, spectroscopic and magnetic study of nanocrystalline Ni–Zn ferrites, Mater. Chem. Phys. 116 (2009) 207–213.
[14] V.A.M. Brabers, Infrared Spectra of cubic and tetragonal manganese ferrites, Phys. Status Solidi B 33 (1969) 563–572.
[15] E.K. Nyutu, W.C. Conner, S.M. Auerbach, C.H. Chen, S.L. Suib, Ultrasonic nozzle spray in situ mixing and microwave-assisted preparation of nanocrystalline spinel metal oxides: nickel ferrite and zinc aluminate, J. Phys. Chem. 112 (2008) 1407–1414.
[16] K. Maaz, S. Karim, A. Mumtaz, S.K. Hasanain, J. Liu, J.L. Duan, Synthesis and magnetic characterization of nickel ferrite nanoparticles prepared by co-precipitation route, J. Magn. Magn. Mater. 321 (2009) 1838–1842.
[17] S.S. Umare, R.S. Ningthoujam, S.J. Sharma, S. Shrivastava, S. Kurian, N.S. Gajbhiye, Mössbauer and magnetic studies on nanocrystalline $NiFe_2O_4$ particles prepared by ethylene glycol route, Hyperfine Interact. 184 (2008) 235–243.
[18] K. Maaz, A. Mumtaz, S.K. Hasanain, A. Ceylan, Synthesis and magnetic properties of cobalt ferrite ($CoFe_2O_4$) nanoparticles prepared by wet chemical route, J. Magn. Magn. Mater. 308 (2007) 289–295.
[19] Z. Gu, X. Xiang, G. Fan, F. Li, Facile synthesis and characterization of cobalt ferrite nanocrystals via a simple reduction-oxidation route, J. Phys. Chem. C 112 (2008) 18459–18466.
[20] L. Ai, J. Jiang, Influence of annealing temperature on the formation, microstructure and magnetic properties of spinel nanocrystalline cobalt ferrites, Curr. Appl. Phys. 10 (2010) 284–288.
[21] M. Atif, S.K. Hasanain, M. Nadeem, Magnetization of sol–gel prepared zinc ferrite nanoparticles: effects of inversion and particle size, Solid State Commun. 138 (2006) 416–421.
[22] S. Ammar, N. Jouini, F. Fiévet, Z. Beji, L. Smiri, P. Moliné, M. Danot, J.M. Grenèche, Magnetic properties of zinc ferrite nanoparticles synthesized by hydrolysis in a polyol medium, J. Phys.: Condens. Matter 18 (2006) 9055–9069.
[23] B. Aslibeiki, P. Kameli, H. Salamati, M. Eshraghi, T. Tahmasebi, Superspin glass state in $MnFe_2O_4$ nanoparticles, J. Magn. Magn. Mater. 322 (2010) 2929–2934.
[24] M.P. Morales, S. Veintemillas-Verdaguer, M.I. Montero, C.J. Serna, A. Roig, L. Casas, B. Martínez, F. Sandiumenge, Surface and internal spin canting in γ-Fe_2O_3 nanoparticles, Chem. Mater. 11 (1999) 3058.
[25] V.A.M. Brabers, in: K.H.J. Buschow (Ed.), Handbook of Magnetic Materials, vol. 8, Elsevier Science, New York, 1995, pp. 197–212 pp..
[26] J. Nogues, I.K. Schuller, Exchange bias, J. Magn. Magn. Mater. 192 (1999) 203–232.
[27] J. Nogues, J. Sort, V. Langlias, et al., Exchange bias in nanostructures, Phys. Rep. Rev. Sect. Phys. Lett. 422 (3) (2005) 65–117.
[28] M. Ghosh, G. Lawes, A. Gayen, G.N. Subbanna, W.M. Reiff, M.A. Subramanian, A.P. Ramirez, J.-P. Zhang, R. Seshadri, A novel route to toluene-soluble magnetic oxide nanoparticles: aqueous hydrolysis followed by surfactant exchange, Chem. Mater. 16 (2004) 118–124.
[29] C.R. Vestal, Z.J. Zhang, effects of surface coordination chemistry on the magnetic properties of $MnFe_2O_4$ spinel ferrite nanoparticles, J. Am. Chem. Soc. 125 (2003) 9828–9833.
[30] S.N. Sidorov, L.M. Bronstein, V.A. Davankov, M.P. Tsyurupa, S.P. Solodovnikov, P.M. Valetsky, E.A. Wilder, R.J. Spontak, Cobalt nanoparticle formation in the pores of hyper-crosslinked polystyrene: control of nanoparticle growth and morphology, Chem. Mater. 11 (1999) 3210–3215.
[31] G. Vaidyanathana, S. Sendhilnathan, Characterization of Co1_xZnxFe_2O_4 nanoparticles synthesized by co-precipitation method, Physica B 403 (2008) 2157–2167.